Advanced Steel Construction – Vol. 18 No. 2 (2022) 561–573
DOI:10.18057/IJASC.2022.18.2.5

EXPERIMENTAL INVESTIGATION OF MECHANICAL BEHAVIOR OF GRADE 8.8 AND 10.9 SMALL-SIZED (M14-M20) BOLTS WITH THE THREAD INTO THE BOLT HOLE

Yang Zhao [1], Zhan Guo [1], Xiao-Lei Xue [1], Quan Lin [1], Yu Chen [1,*] and Geng-Pei Zhang [2,*]

[1] *College of Civil Engineering, Fuzhou University, Fuzhou, China*
[2] *China Three Gorges University, Yichang, China*
** (Corresponding author: E-mail: yuchen@fzu.edu.cn; judgebill@126.com)*

ABSTRACT

This paper is a study on the mechanical behavior of grade 8.8 and 10.9 small-sized (M14-M20) bolts with the thread into the bolt hole. A total of eighty specimens with different thread depth, surface treatment, bolt diameter, and bolt strength grade were subjected to static loading tests. The effects of different parameters on the properties of specimens such as ultimate bearing capacity, initial slip load, ductility, and initial stiffness were systematically investigated. It was demonstrated that the typical failure mode is bolt shear failure. The increase in thread depth causes the ultimate bearing capacity of bolted connections to decrease, and other design parameters also have effects on the ultimate bearing capacity. The ultimate bearing capacity of bolted connections with shot-blasted surfaces is greater than that of bolted connections with wire-brushed surfaces. Moreover, bolted connections with a greater thread depth have a lower yield strength. The method of contact surface treatment, bolt diameter, and strength grade also affect the yield load of bolted connections. The initial stiffness does not change much with the increase of the thread depth. In addition, the increase in thread depth decreases the ductility coefficient and ultimate displacement, which has a negative effect on deformation performance, and the ductility coefficient of bolted connections also decreases with the increase in bolt grade. Finally, based on the test results, a design formula for predicting the ultimate bearing capacity was proposed, and the calculation results match the experimental results well. The difference in ultimate bearing capacity due to thread depth can be well described by the formula.

ARTICLE HISTORY

Received: 15 May 2021
Revised: 24 July 2021
Accepted: 17 September 2021

KEYWORDS

Bolt thread;
Slip resistance;
Ultimate bearing capacity;
Ultimate displacement;
Modified formula

1. Introduction

The commonly connection methods of steel structures include weld connections, bolted connections, and rivet connections. Bolted connections have the advantages of simple construction and detachable, and are widely used in construction engineering. The forms of forces on bolted connections in different applications include shear, tension, and combined action [2]. The failure of steel structures is often caused by connection damage, and the fatigue failure of bolted connections is prone to loss of life and property as there is no significant deformation prior to failure [3]. Compared with ordinary bolts, high-strength bolted connections have greater pre-tightening force, enabling bolts and nuts to effectively clamp the connection plates, resulting in greater friction when subjected to shear. High-strength bolts the advantages of convenient installation, high bearing capacity, and good fatigue resistance [4]. In construction engineering, it often happens that the bolt threads enter the bolt holes. For example, in the process of steel structure installation, sometimes both partially threaded bolts and fully threaded bolts can connect the members, and workers may choose fully threaded bolts at this time. Although a series of researches have been conducted on bolted connections in the past, there is less research on the effect of the depth of bolt threads into the bolt hole on the mechanical behaviors.

High-strength bolted connections can be divided into two categories according to their failure criteria: frictional high-strength bolted connections and pressure-bearing high-strength bolted connections. Frictional high-strength bolted connections are based on the load-bearing limit of relative misalignment sliding and frictional surface damage occurring in the plates. During the service period, the shear force of the frictional high-strength bolted connection should not exceed the maximum frictional force, and the plates should not slip relative to each other. Improper installation of the bolted connection or improper surface treatment of the plate can affect the strength of the frictional bolted connection. Kim et al. [5] investigated the pressure-bearing performance of single-hole and double-hole steel plates, and Kim concluded that the tensile strength of steel plates can better reflect the end tearing failure than the yield strength. Rex et al. [6] tested the pressure-bearing performance of single-hole steel plates and obtained the relationship curve between bolt hole deformation and load, and predicted the strength and initial stiffness.

In multi-bolt connections, Kulak et al. [7] proposed a block shear failure bearing capacity correction formula derived from the existing block shear failure tests and current code formulas. In addition, Shi et al. [8] proposed a simplified model of load versus displacement of high-strength bolts. Annan [9, 10] investigated the slip coefficient of high-strength bolted connections of galvanized weathering steel under tension or compression, and pointed out that the plating thickness and the form of loading had little effect on the slip coefficient. Wang et al. [11] investigated the influences of end distance, and steel grade on failure mode, bearing capacity, and peak displacement through tensile tests on high-strength steel shear connections. Cruz et al. [12] tested the slip coefficient of high-strength bolted connections of S275, S355, and S690 steels with different surface treatment methods, and the results showed that the surface treatment methods had a remarkable effect on the slip coefficient, while the effect of steel grade had a smaller effect on the slip coefficient. Stocchi et al. [13] explored the effects of bolt pre-tension, slip coefficient, and the distance between bolt rod and hole wall on the mechanical properties of bolted connections. The effect of different plate thickness and edge distance on the mechanical properties of bolted connections has also been studied by finite element analysis [14]. Xu et al. [15] conducted shear tests of ordinary bolt threads extending into the bolt hole. The test results showed that for grade 4.8 ordinary bolts, the ultimate bearing capacity of bolted connections gradually decreased as the depth of the thread into the bolt hole increased. Ahmed et al. [16] investigated the effect of threads on the stiffness of bolted connections by finite element analyses.

The previous studies have mostly focused on the effects of end distance and edge distance on the mechanical properties of bolted connections, but there are few studies on the depth of thread entering the bolt hole. In this paper, the thread depth, the surface treatment of the contact surface, the bolt diameter, and the bolt grade are considered, and the load-displacement curve and the strain intensity distribution curve are obtained through the test results. Finally, the design formula for predicting the shear capacity of bolted connections is proposed.

2. Experimental program

2.1. Specimens

Uniaxial static tensile tests were carried out on 80 specimens to assess the shear resistance of bolted connections. Each specimen was composed of a bolt, two connecting plates, and two auxiliary plates. The schematic diagrams of specimens are illustrated in Fig. 1. The size of the connecting plate is 290mm×120mm×12mm. In order to prevent the phenomenon that the testing machine could not completely clamp the specimen, an auxiliary plate of size 120mm×120mm×12mm is welded at the end of the connecting plate. To facilitate the installation of bolts, the selection of bolt hole diameter d_0 is based on the medium assembly in the Chinese Standard "Fasteners-Clearance holes

for bolts and screws" (GB/T 5277-1985) [17]. The bolt hole diameters are 15.5mm, 17.5mm, 20.0mm, and 22.0mm, respectively.

The design of the connecting plate was based on the following three factors. In the parallel direction to the force, when the distance between the bolt hole and the plate end is small, it is easy to lead to the shear failure at the plate end along the direction of the maximum shear stress. In this test, the end distance of the connecting plate is designed to be 3.0d~4.3d to ensure that the connecting plate will not be damaged by the bolt punching and shearing at the end [18]. In the perpendicular to the force direction, when the distance between the bolt hole and the edge of the plate is small, the strength failure of the steel plate along the net section may occur [19]. To ensure the bearing capacity of the steel plate, the edge distance is 3.0d~4.3d. In the selection of the plate thickness, this paper is primarily focused on the bearing capacity of the bolt. Therefore, the designed shear bearing capacity of the bolt in the specimen is less than that of the hole wall. The bearing capacity of the hole wall is associated with the thickness of the plate [20], which is designed to be 12 mm to assure an adequate bearing capacity of the hole wall.

To examine the effect of the thread depth on the mechanical behavior of the bolted connections, five thread depth values of 0 mm, 6 mm, 12 mm, 18 mm, and 24 mm were selected as design parameters for bolted connections. In addition, the bolt grade in this paper is Chinese GB grade.

In summary, the design parameters of this test are as follows：

- The depth of the thread into the bolt hole (l_t):0, 6, 12, 18, and 24 mm.
- Surface treatment: shot-blasted surfaces and wire-brushed surfaces.
- Bolt diameter: M14, M16, M18 and M20.
- Bolt strength grade: 8.8 and 10.9.

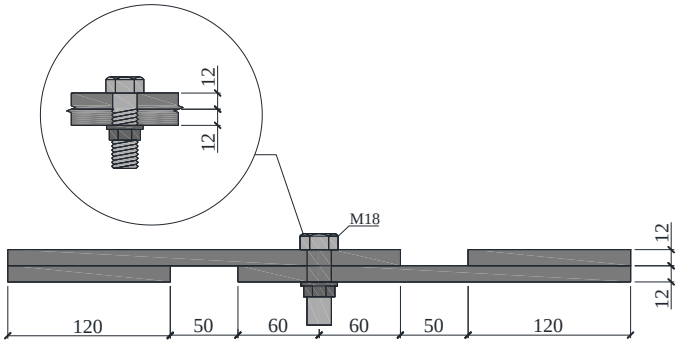

(a) Front view of specimen (The depth of the thread into the hole is 12mm)

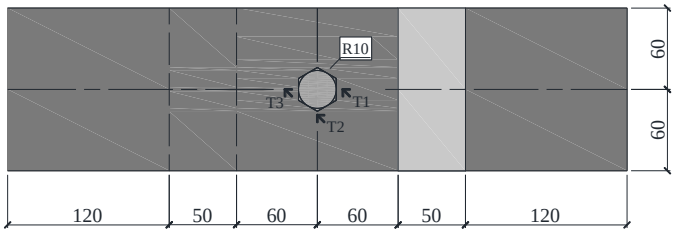

(b) Vertical view of side A and arrangement of strain rosettes

Fig. 1 Schematic diagram of specimen geometry (all dimensions are mm).

2.2. Specimen labeling

To facilitate the identification of the parameters of specimens, all specimens were labeled according to the bolt diameter, bolt strength grade, surface treatment, and thread depth, as shown in Table 1. "SB" or "WB" indicates that the surface treatment is shot-blasted surface or wire-brushed surface. For example, the label "M20-8.8-SB-24-12" is specified as follows:

- "M20" presents that the bolt diameter is 20mm.
- "8.8" presents that the bolt grade is 8.8.
- "SB" means that the surface treatment is shot-blasted surface.
- "24-12" denotes that the total depth of the bolt hole is 24mm and thread depth is 12mm.

2.3. Tightening torque of the bolt

In this test, the torque wrench is used to exert a tightening torque to bolts. The tightening torque of the bolt is determined by the following formula [21]

$$T = kPd \tag{1}$$

where T is the tightening torque, k is the torque coefficient provided by the bolt manufacturer, which is set to 0.130, d is the nominal diameter of the bolt. To minimize the loss of tightening torque, this test was performed soon after the specimen was assembled. The bolt initial torque value is shown in Table 2.

Table 1
Summary of specimens

Specimen labels	Bolt diameter	Bolt grade	Surface treatment	l_t (mm)
M14-8.8-WB-24-0	M14	8.8	wire-brushed	0
M14-8.8-WB-24-6	M14	8.8	wire-brushed	6
M14-8.8-WB-24-12	M14	8.8	wire-brushed	12
M14-8.8-WB-24-18	M14	8.8	wire-brushed	18
M14-8.8-WB-24-24	M14	8.8	wire-brushed	24
M14-8.8-SB-24-0	M14	8.8	shot-blasted	0
M14-8.8-SB-24-6	M14	8.8	shot-blasted	6
M14-8.8-SB-24-12	M14	8.8	shot-blasted	12
M14-8.8-SB-24-18	M14	8.8	shot-blasted	18
M14-8.8-SB-24-24	M14	8.8	shot-blasted	24
M14-10.9-WB-24-0	M14	10.9	wire-brushed	0
M14-10.9-WB-24-6	M14	10.9	wire-brushed	6
M14-10.9-WB-24-12	M14	10.9	wire-brushed	12
M14-10.9-WB-24-18	M14	10.9	wire-brushed	18
M14-10.9-WB-24-24	M14	10.9	wire-brushed	24
M14-10.9-SB-24-0	M14	10.9	shot-blasted	0
M14-10.9-SB-24-6	M14	10.9	shot-blasted	6
M14-10.9-SB-24-12	M14	10.9	shot-blasted	12
M14-10.9-SB-24-18	M14	10.9	shot-blasted	18
M14-10.9-SB-24-24	M14	10.9	shot-blasted	24
M16-8.8-WB-24-0	M16	8.8	wire-brushed	0
M16-8.8-WB-24-6	M16	8.8	wire-brushed	6
M16-8.8-WB-24-12	M16	8.8	wire-brushed	12
M16-8.8-WB-24-18	M16	8.8	wire-brushed	18
M16-8.8-WB-24-24	M16	8.8	wire-brushed	24
M16-8.8-SB-24-0	M16	8.8	shot-blasted	0
M16-8.8-SB-24-6	M16	8.8	shot-blasted	6
M16-8.8-SB-24-12	M16	8.8	shot-blasted	12
M16-8.8-SB-24-18	M16	8.8	shot-blasted	18
M16-8.8-SB-24-24	M16	8.8	shot-blasted	24
M16-10.9-WB-24-0	M16	10.9	wire-brushed	0
M16-10.9-WB-24-6	M16	10.9	wire-brushed	6
M16-10.9-WB-24-12	M16	10.9	wire-brushed	12
M16-10.9-WB-24-18	M16	10.9	wire-brushed	18
M16-10.9-WB-24-24	M16	10.9	wire-brushed	24
M16-10.9-SB-24-0	M16	10.9	shot-blasted	0
M16-10.9-SB-24-6	M16	10.9	shot-blasted	6
M16-10.9-SB-24-12	M16	10.9	shot-blasted	12
M16-10.9-SB-24-18	M16	10.9	shot-blasted	18
M16-10.9-SB-24-24	M16	10.9	shot-blasted	24
M18-8.8-WB-24-0	M18	8.8	wire-brushed	0
M18-8.8-WB-24-6	M18	8.8	wire-brushed	6
M18-8.8-WB-24-12	M18	8.8	wire-brushed	12
M18-8.8-WB-24-18	M18	8.8	wire-brushed	18
M18-8.8-WB-24-24	M18	8.8	wire-brushed	24
M18-8.8-SB-24-0	M18	8.8	shot-blasted	0

M18-8.8-SB-24-6	M18	8.8	shot-blasted	6
M18-8.8-SB-24-12	M18	8.8	shot-blasted	12
M18-8.8-SB-24-18	M18	8.8	shot-blasted	18
M18-8.8-SB-24-24	M18	8.8	shot-blasted	24
M18-10.9-WB-24-0	M18	10.9	wire-brushed	0
M18-10.9-WB-24-6	M18	10.9	wire-brushed	6
M18-10.9-WB-24-12	M18	10.9	wire-brushed	12
M18-10.9-WB-24-18	M18	10.9	wire-brushed	18
M18-10.9-WB-24-24	M18	10.9	wire-brushed	24
M18-10.9-SB-24-0	M18	10.9	shot-blasted	0
M18-10.9-SB-24-6	M18	10.9	shot-blasted	6
M18-10.9-SB-24-12	M18	10.9	shot-blasted	12
M18-10.9-SB-24-18	M18	10.9	shot-blasted	18
M18-10.9-SB-24-24	M18	10.9	shot-blasted	24
M20-8.8-WB-24-0	M20	8.8	wire-brushed	0
M20-8.8-WB-24-6	M20	8.8	wire-brushed	6
M20-8.8-WB-24-12	M20	8.8	wire-brushed	12
M20-8.8-WB-24-18	M20	8.8	wire-brushed	18
M20-8.8-WB-24-24	M20	8.8	wire-brushed	24
M20-8.8-SB-24-0	M20	8.8	shot-blasted	0
M20-8.8-SB-24-6	M20	8.8	shot-blasted	6
M20-8.8-SB-24-12	M20	8.8	shot-blasted	12
M20-8.8-SB-24-18	M20	8.8	shot-blasted	18
M20-8.8-SB-24-24	M20	8.8	shot-blasted	24
M20-10.9-WB-24-0	M20	10.9	wire-brushed	0
M20-10.9-WB-24-6	M20	10.9	wire-brushed	6
M20-10.9-WB-24-12	M20	10.9	wire-brushed	12
M20-10.9-WB-24-18	M20	10.9	wire-brushed	18
M20-10.9-WB-24-24	M20	10.9	wire-brushed	24
M20-10.9-SB-24-0	M20	10.9	shot-blasted	0
M20-10.9-SB-24-6	M20	10.9	shot-blasted	6
M20-10.9-SB-24-12	M20	10.9	shot-blasted	12
M20-10.9-SB-24-18	M20	10.9	shot-blasted	18
M20-10.9-SB-24-24	M20	10.9	shot-blasted	24

Table 2
The bolt initial torque value P (kN)

Bolt grade	Bolt diameter			
	M14	M16	M18	M20
8.8	120	183	245	358
10.9	150	228	309	443

2.4. Material properties

The connecting plates and auxiliary plates of this test were made of Q345 steel. According to the requirements of the Chinese Standard of Test Pieces For Mechanical Testing (GB/T 2975-2018) [22] and Metallic Materials (GB/T 228-2010) [23], tensile tests were performed to obtain the mechanical characteristics of the steel. The specific mechanical characteristics are shown in Table 3.

Table 3
Summary of steel properties

Component	Elastic modulus E (GPa)	Poisson's ratio v	Yield strength f_y (MPa)	Tensile strength f_u (MPa)
Connecting plate	206	0.30	385	524

2.5. Experimental device and procedures

As illustrated in Fig. 2, The axial tension experiments were performed using a universal test machine (UTM) with a range of 500kN. The specimens were installed in accordance with the experimental requirements, as plotted in Fig. 3. During the installation of the specimen, the digital torque wrench was employed to exert torque on bolts. The torque wrench has a range of 42.5N·m-850N·m with an accuracy of 2.5%. Subsequently, the specimen was positioned in the center of the two fixtures of the universal testing machine to enable the central line of specimens to be aligned with the direction of load. The specimen was clamped with two fixtures and then stretched vertically, and the schematic diagram of test loading is illustrated in Fig. 4. Before the test, the data acquisition system (DH3816) was adjusted to balance the strain acquisition and guarantee the accuracy of the experimental result [24]. The specimens were applied slowly at a loading rate of 0.3kN/s to ensure the precision of the test data [25]. The tensile test was terminated when the specimen was damaged. In the course of loading, the testing machine can accurately record the load and the corresponding displacement.

To evaluate the characteristics of the strain distribution of the plate around the hole wall, a total of ten typical specimens (M14-8.8-SB-24-12, M16-8.8-SB-24-12, M18-8.8-SB-24-0, M18-8.8-SB-24-6, M18-8.8-SB-24-12, M18-8.8-SB-24-18, M18-8.8-SB-24-24, M18-8.8-WB-24-12, M18-10.9-SB-24-12, M20-8.8-SB-24-12) were picked for strain measurement. In each test specimen, a total of six strain gauges (T1-T6) were positioned on the plate around the hole wall to record the strain distribution, as illustrated in Fig. 1(b) and (c). The DH3816 strain acquisition system regularly measures the strain data from all measuring points [26].

(a) All device photo (b) Details of experimental setup

Fig. 2 Experimental setup

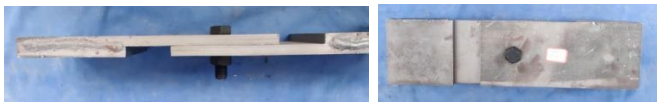

(a) Front view of specimen (b) Vertical view of side A

Fig. 3 Assembled specimen

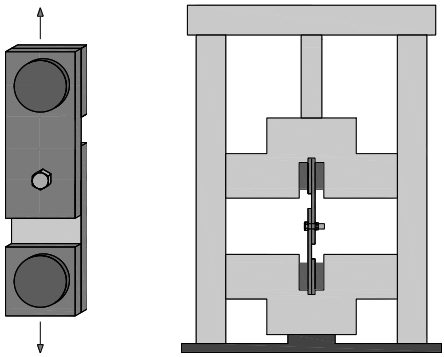

Fig. 4 Schematic diagram of loading process

3. Test results and analysis

3.1. Failure modes

All specimens presented some similar failure characteristics under

shearing action, and the typical failure mode is bolt shear failure. It is observed that bolt shear deformation is remarkable during the loading process. At the beginning of loading, the bolt did not show significant shear deformation until the load approached 65% of the ultimate load. When the load approximated the ultimate load, the shear deformation of the bolt increased greatly, and the steel plate deformed around the hole wall. Depending on the phenomenon of the bolt shear failure, the failure modes can be classified further into two categories: bolt failure, and bolt and thread failure, as plotted in Fig. 5. The experimental results are shown in Table 4. The specific explanation of failure modes is as described below:

(1) Failure mode 1: the shear failure appeared in the unthreaded section of the bolt and slight deformation of the steel plate around the hole wall. In the unthreaded section of the bolt, and the steel plate showed slight deformation around the hole wall. In this case, the bolt failure surface was relatively smooth, and the angle of the failure surface was close to the horizontal plane, as plotted in Fig. 5(a) and (b). This failure mode occurred in the specimen with the thread depth of 0, 6 mm in the experiment. The bolt was subjected to the maximum tangential stress at the contact surface of the two connecting plates, causing the bolt failure surface to pass through the contact surface. In this case, the maximum tangential stress was applied to the unthreaded section.

(2) Failure mode 2: the shear failure appeared in the threaded section of the bolt, and the hole wall deformation was similar to failure mode 1. The bolt failure surface was relatively rough, and the failure surface passed through the contact surface of the two connecting plates and along the thread direction, as illustrated in Fig. 5(c) and (d). This failure mode occurred in the specimen with the thread depth of 12, 18, and 24mm in the experiment. When the boundary between the threaded section and the unthreaded section passed through the plate contact surface, the bolt failure surface appeared in the threaded section because the net cross-sectional area of the threaded part of the bolt is smaller than that of the unthreaded area, and the shear strength of the threaded section is lower than that of the unthreaded section.

Table 4
Experimental results for all specimens

Specimen label	P_{us} (kN)	P_y (kN)	P_u (kN)	μ	k_i (kN/mm)	Δ_u (mm)
M14-8.8-WB-24-0	16.77	55.83	59.77	2.05	294.44	3.98
M14-8.8-WB-24-6	16.36	52.56	57.05	1.80	286.39	4.31
M14-8.8-WB-24-12	17.16	50.10	53.47	1.76	280.43	4.99
M14-8.8-WB-24-18	16.04	46.51	48.35	1.72	304.95	2.98
M14-8.8-WB-24-24	17.10	40.86	43.38	1.66	295.86	2.90
M14-8.8-SB-24-0	27.50	62.68	65.28	1.75	333.56	3.48
M14-8.8-SB-24-6	28.03	59.40	62.33	1.71	334.63	3.28
M14-8.8-SB-24-12	26.57	55.69	57.90	1.56	332.91	3.08
M14-8.8-SB-24-18	27.16	51.16	53.19	1.50	321.65	2.74
M14-8.8-SB-24-24	27.23	47.04	48.67	1.43	348.89	2.47
M14-10.9-WB-24-0	20.21	69.21	71.92	1.87	222.49	3.36
M14-10.9-WB-24-6	18.61	67.54	69.77	1.60	222.37	3.51
M14-10.9-WB-24-12	18.90	59.38	62.64	1.42	235.29	2.78
M14-10.9-WB-24-18	17.01	56.36	58.08	1.35	226.50	2.67
M14-10.9-WB-24-24	18.14	49.90	51.84	1.32	232.00	2.69
M14-10.9-SB-24-0	32.88	77.31	82.14	2.01	207.62	3.85
M14-10.9-SB-24-6	31.93	73.84	77.77	1.95	204.45	3.47
M14-10.9-SB-24-12	30.58	70.72	73.87	1.68	204.80	3.27
M14-10.9-SB-24-18	31.55	63.24	64.65	1.27	201.17	3.08
M14-10.9-SB-24-24	31.22	52.96	54.01	1.22	216.36	2.44
M16-8.8-WB-24-0	24.30	69.22	75.82	2.36	326.13	3.49
M16-8.8-WB-24-6	23.84	68.89	72.13	1.73	321.05	3.14
M16-8.8-WB-24-12	22.70	63.27	66.42	1.53	333.58	2.98
M16-8.8-WB-24-18	24.87	55.81	59.48	1.44	318.62	2.30
M16-8.8-WB-24-24	24.60	55.23	56.09	1.41	328.14	2.28
M16-8.8-SB-24-0	36.22	82.41	87.66	2.06	249.54	3.90
M16-8.8-SB-24-6	34.73	77.10	81.50	1.88	267.30	3.46
M16-8.8-SB-24-12	35.89	71.29	75.70	1.83	245.56	3.93
M16-8.8-SB-24-18	33.03	60.74	65.65	1.78	288.30	2.66
M16-8.8-SB-24-24	33.04	60.87	63.84	1.69	261.54	2.87
M16-10.9-WB-24-0	29.45	88.41	92.72	1.90	316.27	3.56
M16-10.9-WB-24-6	30.69	81.88	86.59	1.88	343.64	3.34
M16-10.9-WB-24-12	29.66	76.37	80.03	1.50	333.14	2.12
M16-10.9-WB-24-18	29.06	66.70	70.02	1.36	310.48	1.86
M16-10.9-WB-24-24	28.62	63.26	63.77	1.30	335.04	2.18
M16-10.9-SB-24-0	45.64	94.66	100.86	2.52	373.26	3.32
M16-10.9-SB-24-6	46.01	94.01	97.69	1.83	339.28	3.26
M16-10.9-SB-24-12	44.53	84.89	88.47	1.50	372.46	2.57
M16-10.9-SB-24-18	45.51	76.98	79.40	1.35	346.19	2.25
M16-10.9-SB-24-24	44.19	73.58	74.46	1.20	353.54	2.38
M18-8.8-WB-24-0	32.81	83.83	95.40	2.58	263.01	4.15
M18-8.8-WB-24-6	31.97	82.65	89.59	1.97	280.21	4.28
M18-8.8-WB-24-12	32.91	80.54	85.26	1.69	260.05	4.64
M18-8.8-WB-24-18	31.42	75.52	77.75	1.31	274.81	2.83
M18-8.8-WB-24-24	31.30	66.00	70.17	1.31	272.69	2.83
M18-8.8-SB-24-0	46.25	95.28	100.73	1.83	215.14	4.72
M18-8.8-SB-24-6	42.26	90.57	95.74	1.78	231.36	5.11
M18-8.8-SB-24-12	43.07	84.73	89.92	1.59	211.39	4.52
M18-8.8-SB-24-18	44.07	81.54	84.51	1.53	224.72	3.79
M18-8.8-SB-24-24	44.00	73.68	77.19	1.37	231.20	3.31
M18-10.9-WB-24-0	37.87	114.51	121.75	1.89	327.14	4.55
M18-10.9-WB-24-6	34.68	110.03	117.14	1.70	330.96	4.13
M18-10.9-WB-24-12	35.44	100.97	105.23	1.37	335.66	3.40
M18-10.9-WB-24-18	37.48	87.28	91.60	1.34	324.85	2.48
M18-10.9-WB-24-24	37.61	81.69	86.29	1.27	335.04	2.01
M18-10.9-SB-24-0	53.02	123.69	131.27	1.85	319.61	4.08
M18-10.9-SB-24-6	53.45	120.09	125.52	1.46	309.82	4.55
M18-10.9-SB-24-12	54.61	107.60	111.70	1.39	307.29	3.95
M18-10.9-SB-24-18	53.47	98.71	101.26	1.26	311.62	2.94
M18-10.9-SB-24-24	51.29	90.02	92.36	1.25	307.81	2.84
M20-8.8-WB-24-0	39.96	101.22	116.44	2.60	313.72	5.24
M20-8.8-WB-24-6	38.84	100.48	111.81	2.28	316.99	5.56
M20-8.8-WB-24-12	39.22	91.30	102.28	2.11	327.38	4.39
M20-8.8-WB-24-18	38.65	81.41	88.36	1.68	294.28	2.92
M20-8.8-WB-24-24	40.30	76.38	80.29	1.62	306.93	3.20
M20-8.8-SB-24-0	56.58	118.50	127.98	1.97	331.00	5.70
M20-8.8-SB-24-6	55.49	112.76	123.17	1.96	347.84	5.32
M20-8.8-SB-24-12	54.74	103.20	109.43	1.87	339.76	6.55
M20-8.8-SB-24-18	55.62	97.66	100.76	1.76	333.60	4.98
M20-8.8-SB-24-24	54.67	88.51	92.39	1.46	342.17	3.16
M20-10.9-WB-24-0	48.90	140.13	146.09	1.76	276.37	4.92
M20-10.9-WB-24-6	43.37	135.67	142.12	1.67	284.31	5.77
M20-10.9-WB-24-12	46.88	116.13	121.69	1.48	263.84	4.15
M20-10.9-WB-24-18	46.43	107.08	112.84	1.34	279.76	3.75
M20-10.9-WB-24-24	49.94	106.36	108.39	1.20	260.10	3.65
M20-10.9-SB-24-0	67.32	153.84	160.87	1.65	241.40	5.37
M20-10.9-SB-24-6	69.06	149.28	156.56	1.60	246.76	4.81
M20-10.9-SB-24-12	69.11	126.90	132.77	1.58	220.98	4.48
M20-10.9-SB-24-18	68.00	120.13	123.23	1.38	229.91	4.21
M20-10.9-SB-24-24	68.42	111.90	116.02	1.24	240.71	4.09

(a) M14-8.8-SB-24-0

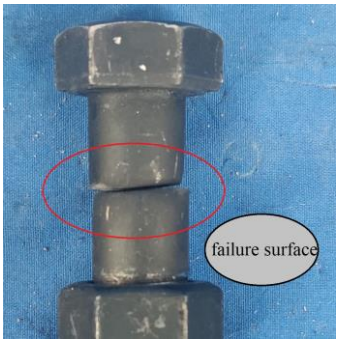

(b) Bolt rod failure

(c) M18-8.8-SB-24-0

(d) Bolt rod failure

(e) M20-10.9-SB-24-18

(f) Bolt rod and thread failure

(g) M18-8.8-SB-24-12

(h) Bolt rod and thread failure

(i) M16-10.9-SB-24-12

(j) M14-10.9-NP-24-18

Fig. 5 Failure mode of specimens

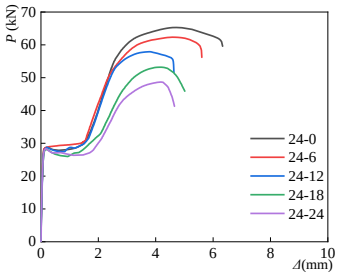

(a) M14-8.8-SB

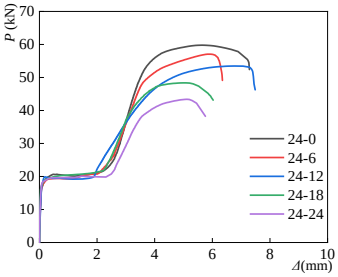

(b) M14-8.8-WB

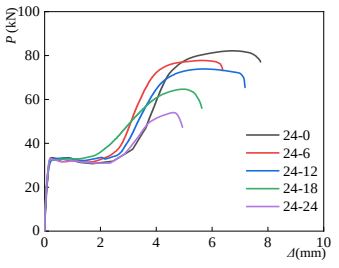

(c) M14-10.9-SB

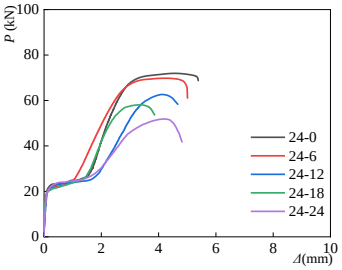

(d) M14-10.9-WB

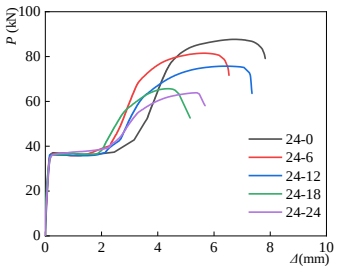

(e) M16-8.8-SB

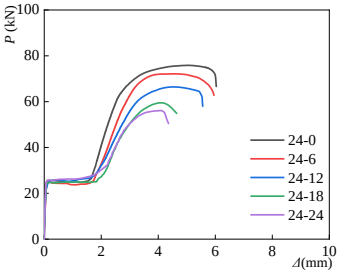

(f) M16-8.8-WB

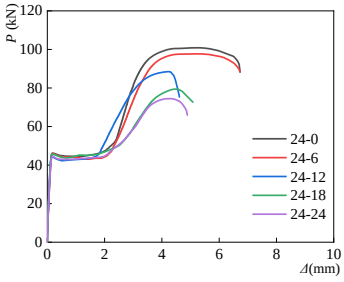

(g) M16-10.9-SB

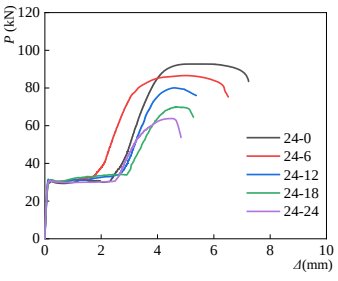

(h) M16-10.9-WB

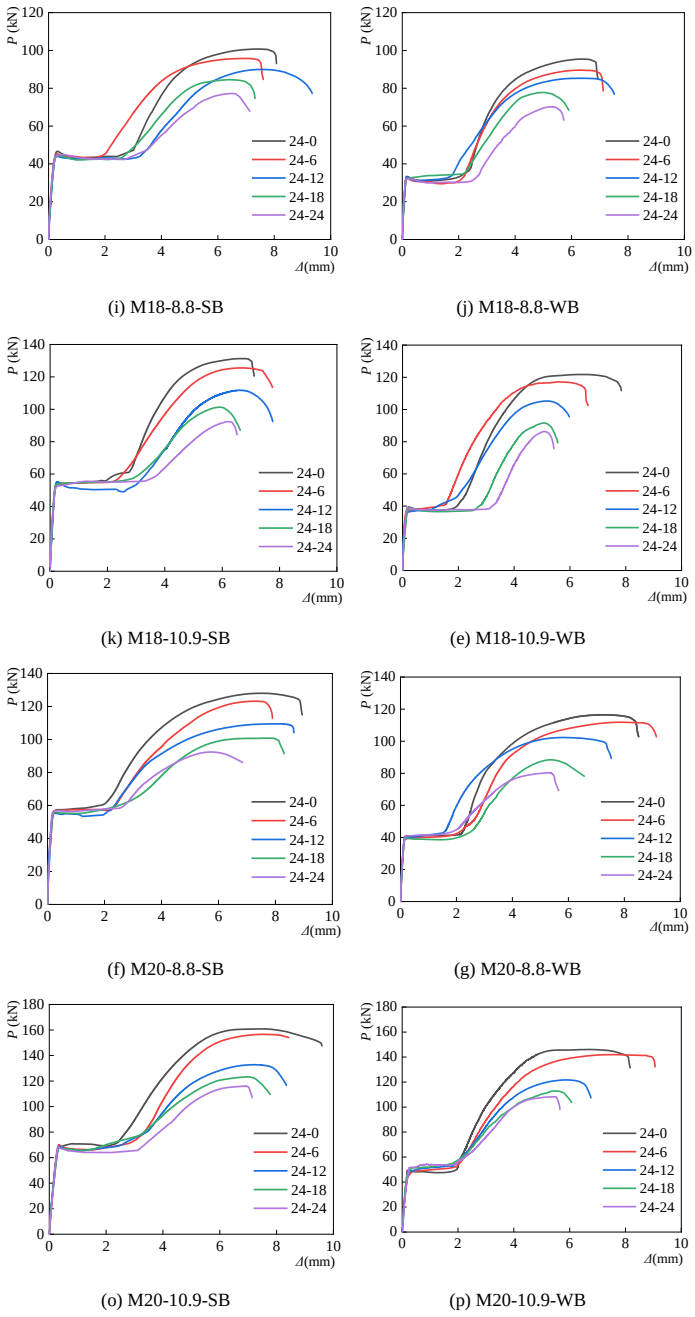

(i) M18-8.8-SB (j) M18-8.8-WB

(k) M18-10.9-SB (e) M18-10.9-WB

(f) M20-8.8-SB (g) M20-8.8-WB

(o) M20-10.9-SB (p) M20-10.9-WB

Fig. 6 Load-displacement curves

3.2. Load-displacement curves

Fig. 6 presents the load-displacement curves of specimens with different thread depths, surface treatments, bolt diameters, and bolt strength grades, respectively. Based on the stress characteristics of bolted connections, the stress process is divided into four stages: friction stage, sliding stage, bolt force transmission stage, and failure stage. Meanwhile, the typical load-displacement curve is depicted in Fig. 7.

(1) Friction stage: this stage was at the preliminary stage of loading. At this time, the load was small, and there was no obvious deformation of bolted connections. The load was transmitted through the frictional between the contact surfaces of the plates. At this stage, the displacement of the specimen was quite small, and the load-displacement curve was an sloping straight, and the specimen was in the elastic phase at this time.

(2) Sliding stage: when the load was above the maximum friction between the contact surfaces of the plates, the contact surfaces would slip relatively. The distance between bolt and hole wall decreased gradually, and finally the bolt and hole wall came into contact, and the stiffness of the joint dropped sharply. The sliding length was composed of two parts, including the gap between the bolt and hole wall and the slight extrusion deformation at the hole wall. The slip length in the load-displacement curves of each specimen was not the same because the bolt was not located at the center of the bolt hole.

(3) Bolt force transmission stage: at this stage, the load was principally transmitted by the contact between the bolt and the hole wall. The hole wall was extruded and deformed, and the bolt was progressively deformed and bent, and the stiffness of the joint increased significantly. As the load increased, the relative displacement between the plates increased continuously.

(4) Failure stage: the relative displacement increased significantly, and bolt was eventually cut into two sections and the bolted connection was damaged. The load reached its maximum value, and then the load-displacement curve began to decrease.

As indicated in Fig. 6, the trends of the displacement-load curves are approximately the same, indicating that the force conditions of the specimens are roughly the same.

The initial slip load is specified as the boundary point between the friction stage and the sliding stage. By observing the displacement-load curves, it can be found that the thread depth has an adverse effect on the ultimate bearing capacity, and which has no significant effect on the initial slip load.

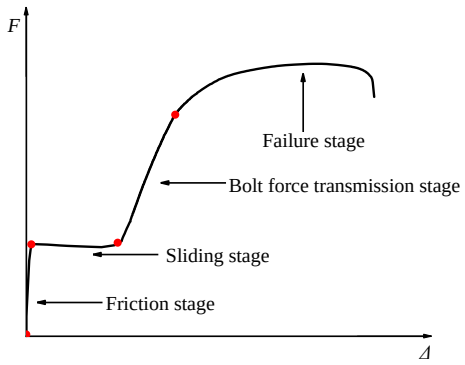

Fig. 7 Typical load-displacement curve

3.3. Initial slip load

Fig. 8 shows the initial slip load of all specimens. When other variables remain unchanged, the difference in initial slip load for different thread depths is generally less than 10%. The results show that the initial slip load does not change significantly with the increase of the thread depth, because the pre-tightening force of bolts does not change with increasing thread depth, and the initial slip load is related to the pre-tightening force of bolts.

The influence of surface treatment on the initial slip load can be found in Fig. 8 and Table 4. Compared with the specimen with wire-brushed surfaces, the average value of the initial slip load of the specimens with shot-blasted surfaces increases by around 50%. This phenomenon indicates that surface treatment methods have a significant effect on the initial slip load. Increasing the roughness of the contact surface can effectively enhance the initial slip load. This is because the surface treatment changes the slip coefficient of the friction surface, and the initial slip load is related to the slip coefficient of the friction surface.

Fig. 8 also shows the impact of bolt diameter and bolt strength grade on the initial slip load. If the bolt diameter ranges from 14 to 16, 18, and 20 mm, the average value of the initial slip load increases by around 42%, 76%, and 123%, respectively. It can be found that increasing the bolt diameter can dramatically raise the initial slip load. If the bolt grade ranges from 8.8 to 10.9, the average value of the initial slip load increases by around 21%. The results indicate that increasing the bolt strength grade can improve the initial slip load. This is because as the bolt diameter and bolt grade increase, the pre-tightening force applied to the bolt gradually increases, thus increasing the pressure between the friction surfaces of the plates, and finally enhancing the initial slip load.

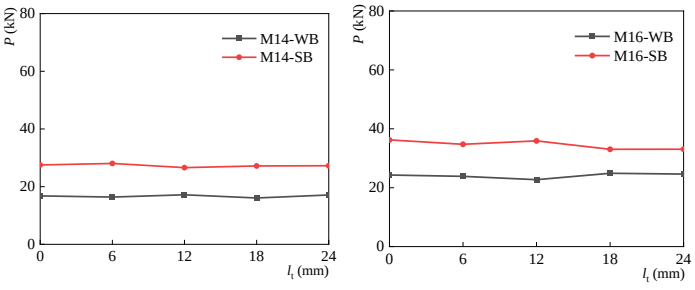

(a) M14-8.8 (b) M16-8.8

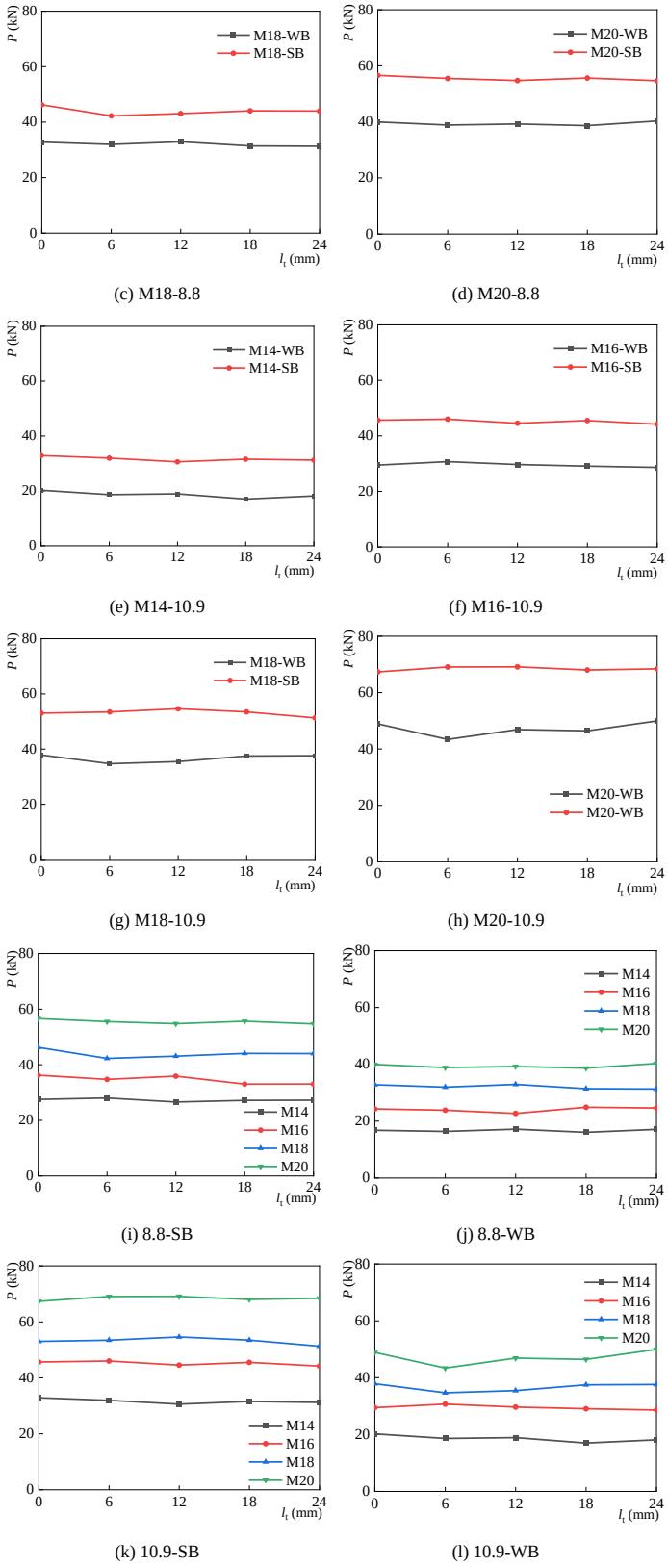

(c) M18-8.8 (d) M20-8.8

(e) M14-10.9 (f) M16-10.9

(g) M18-10.9 (h) M20-10.9

(i) 8.8-SB (j) 8.8-WB

(k) 10.9-SB (l) 10.9-WB

Fig. 8 Initial slip load versus depth thread curves

3.4. Yield load

For the load-displacement curve without obvious yield point, some equivalent methods are needed to determine the yield load. In this paper, geometric drawing method is used. The specific method of geometric drawing method is shown in Fig. 9 [27-28]. In Fig. 9, F_{max} is the ultimate bearing capacity of bolted connections. First, the tangent line oa of the curve is drawn, and then the horizontal line passing through point u is drawn, and the horizontal line and the tangent line oa intersect at point a. Draw the perpendicular to the line au, and the intersection point of the perpendicular line and the curve is point b. Draw extension line ob, and the extension line ob intersects line au at point c. The perpendicular line of au is drawn through point c, and the intersection point of the vertical line and the curve is point y, and point y is the yield point of the specimen.

The influence of the thread depth on the yield load of bolted connections is depicted in Fig. 10. It can be seen that the yield load of specimens is decreased with the increment of the thread depth. For example, specimens M14-8.8-SB-24-6 to M14-8.8-SB-24-24 comparing with M14-8.8-SB-24-0, the yield load of the specimens is reduced by 5.2%, 11.1%, 18.4%, and 24.9%, respectively. If the thread depth ranges from 0 to 6, 12, 18, and 24 mm, the average value of the yield load decreases by around 3.8%, 11.8%, 19.5%, and 25.6%, respectively. When the thread depth ranges from 6 to 24 mm, the average value of the yield load decreases linearly with the increase of thread depth. When the thread depth is 6 mm, the increase of thread depth has little influence on the average value of the yield load.

As demonstrated in Fig. 10, the results demonstrate that the yield strength of bolted connections with shot-blasted treatment on the contact surfaces of the plates is greater than that of bolted connections with wire-brushed surfaces. Compared with bolted connections with wire-brushed surfaces, the average value of the yield load of the specimens with shot-blasted surfaces increases by around 11%. The experimental results also indicate that the yield strength of bolted connections improves when the grade of bolts is increased from 8.8 to 10.9. With the increase of bolt diameter from M14 to M20, the yield strength of the specimens increases gradually.

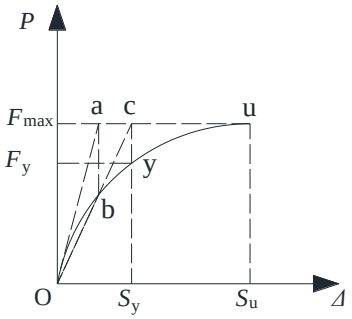

Fig. 9 Geometric drawing method

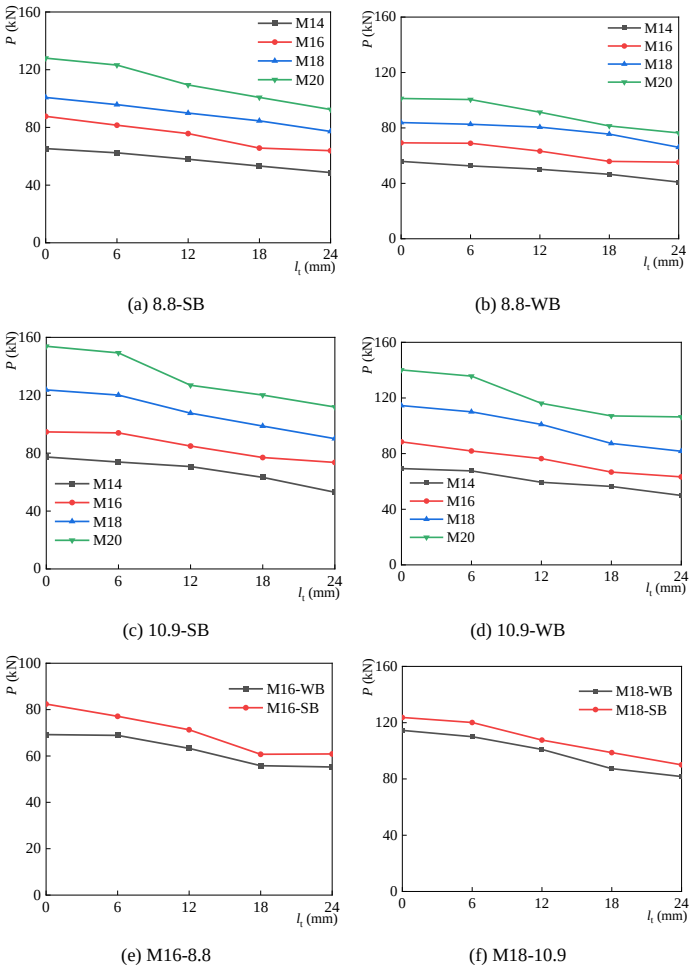

(a) 8.8-SB (b) 8.8-WB

(c) 10.9-SB (d) 10.9-WB

(e) M16-8.8 (f) M18-10.9

Fig. 10 Yield load versus thread depth curves

3.5. Ultimate bearing capacity

Fig. 11 illustrates the effect of thread depth on the ultimate bearing capacity of bolted connections. As demonstrated in Table 4, if the thread depth ranges from 0 to 6, 12, 18, and 24 mm, the average value of the ultimate capacity decreases by around 5%, 13%, 22%, and 28%, respectively. For example, the ultimate bearing capacity of M14-8.8-WB-24-0 without thread entering the hole is 59.77kN, and the ultimate bearing capacity of M14-8.8-WB-24-6 to M14-8.8-WB-24-24 is 57.05kN, 53.47kN, 48.35KN, and 43.38kN respectively. Compared with bolted connections without thread entering the hole, the ultimate bearing capacity is reduced by 5%, 11%, 19%, and 27%, respectively. The test results indicate that as the thread depth increases, the ultimate bearing capacity gradually decreases.

Based on the above explanation in this paper, the increase of thread depth has little impact on the initial slip load, which illustrates that the thread depth slightly affects the friction stage and sliding stage, and mainly affects the bolt force transmission stage and failure stage. When the threads are in contact with the hole wall, the threads decrease the net cross-sectional area of the bolt, which reduces the shear capacity of the bolt and leads to premature failure of the component.

Table 4 and Fig. 12 show the effect of bolt diameter on the ultimate bearing capacity of bolted connections. The ultimate bearing capacity is enhanced with the increment of bolt diameters, regardless of the type of surface treatment. In addition, it is observed that the effect of thread depth and bolt diameter on ultimate bearing capacity is not correlated. For instance, the ultimate bearing capacity of the specimens M14-8.8-SB-24-12 to M20-8.8-SB-24-12 is 57.90N, 75.70KN, 89.92KN, and 109.43KN, respectively. Compared with the specimens without thread entering the bolt hole, the ultimate bearing capacity is reduced by 11.14%, 13.65%, 10.73%, and 14.49%, respectively. The data indicate that the decrease degree of ultimate bearing capacity is not dramatically affected by variations in bolt diameter when the thread depth is the same.

Table 4 and Fig. 6 display the effect of surface treatment on the ultimate bearing capacity of the specimens. It can be observed that the surface treatment has a considerable impact on the ultimate bearing capacity. The ultimate bearing capacity of bolted connections with shot-blasted surfaces is 10% larger than that of bolted connections with wire-brushed surfaces. Likewise, the decrease degree of ultimate bearing capacity is not markedly altered by the change of surface treatment when the thread depth is the same. According to the test results, it is deduced that the influence of surface treatment on the ultimate bearing capacity is related to the initial slip load.

Table 4 and Fig. 6 demonstrate the effect of bolt grade on the ultimate bearing capacity of the specimens. If the bolt grade ranges from 8.8 to 10.9, the average value of the ultimate bearing capacity increases by 23%. The results illustrate that the ultimate bearing capacity is enhanced as the bolt strength grade increases, regardless of the type of surface treatment and bolt diameter. Similarly, the change of bolt strength grade has no significant effect on the percentage decrease of ultimate bearing capacity caused by thread entering the hole.

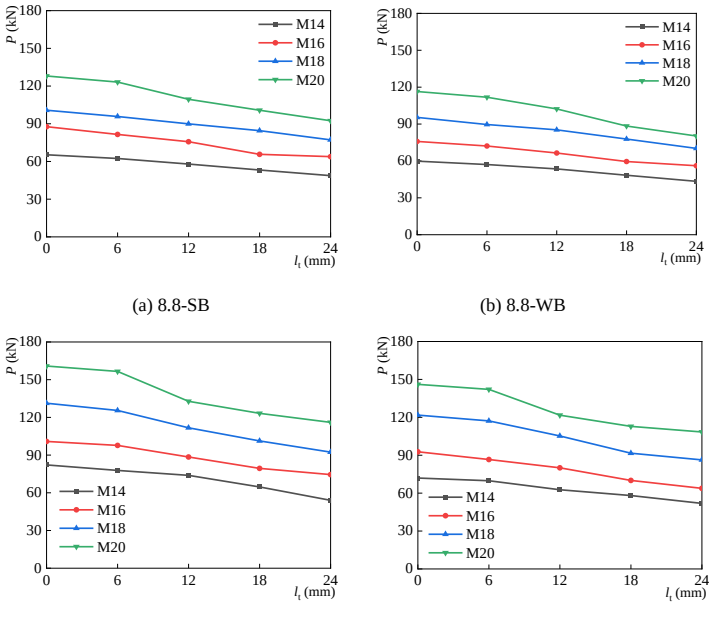

(a) 8.8-SB (b) 8.8-WB

(c) 10.9-SB (d) 10.9-WB

Fig. 11 Ultimate bearing capacity versus thread depth curves

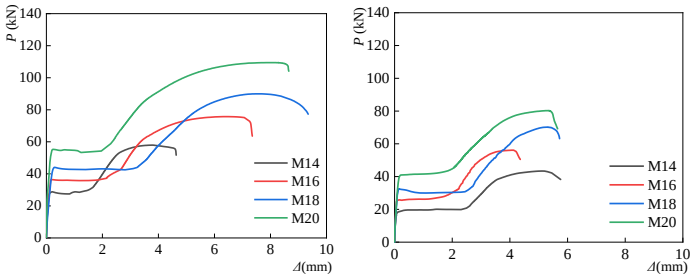

(a) 8.8-SB-24-12 (b) 8.8-WB-24-24

Fig. 12 Load-displacement curves of different bolt diameters at the same thread depth

3.6. Initial stiffness

The initial stiffness is the slope of the load-displacement curve in the elastic stage. Table 4 shows the initial stiffness of bolted connections. Fig. 13 illustrates the elastic stage of the load-displacement curve of specimens M16-8.8-WB and M20-10.9-SB. If the thread depth ranges from 0 to 6, 12, 18, and 24 mm, the initial stiffness is 326.13, 321.05, 333.58, 318.62, and 328.14kN/mm, respectively. When other variables remain unchanged, the difference in the initial stiffness for different thread depths is generally less than 10%. The results show that the initial stiffness does not change much with the increase of the thread depth. This is because the bolt and the hole wall are not in contact at the elastic stage, so the depth of the thread has no direct effect on the initial stiffness. In addition, the test results show that the surface treatment, bolt diameter, and bolt strength grade have no noticeable effect on the initial stiffness.

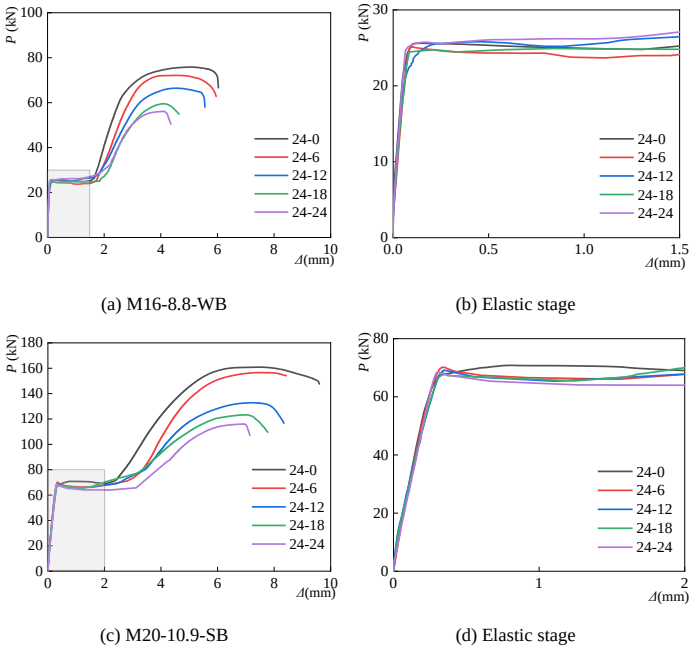

(a) M16-8.8-WB (b) Elastic stage

(c) M20-10.9-SB (d) Elastic stage

Fig. 13 Initial stiffness

3.7. Ductility coefficient and ultimate displacement

Ductility is the plastic deformation ability of a structure, a component, or a section of a component from the beginning of yielding to the failure stage. It is an important indicator of seismic performance of the structure. Ductility coefficient is defined as the ratio of the ultimate displacement to yield displacement of the specimens, and the calculation formula is represented as

$$u = \frac{\Delta_u}{\Delta_y} \tag{2}$$

Where Δ_u is the ultimate displacement, and Δ_y is the yield displacement.

Based on the formula, the ductility coefficient is displayed in Table 4 and the influence of the thread depth on the ductility coefficient is shown in Fig. 14. if the thread depth ranges from 0 to 6, 12, 18, and 24 mm, the average value of

ductility coefficient decreases by around 12%, 21%, 28%, and 32%, respectively. The overall trend shows that an increase in thread depth will decrease the ductility coefficient of bolted connections. Moreover, the growth rate of the decrease in the ductility coefficien gradually slows down when the thread depth increases from 0 to 24mm.

Fig. 14 also displays the effect of bolt grade on the ductility coefficient of bolted connections. It can be found that the average ductility coefficient of the specimens with bolt strength grade of 10.9 is 13% lower than that of the specimens with the bolt strength grade of 8.8 ($u_{8.8}$=1.77, $u_{10.9}$=1.55). The results indicate that the increase of bolt strength grade will reduce the ductility coefficient of the specimens. Furthermore, the test results show that the bolt diameter and surface treatment exert little effect on the ductility coefficient of bolted connections.

The effects of thread depth, surface treatment, bolt diameter, and bolt strength grade on the ultimate displacement are indicated in Fig. 15. It is observed that the ultimate displacement of the specimens with thread depth of 18mm and 24mm is less than those of the specimens with thread depth of 0mm and 6mm, indicating that the increase of thread depth can decrease the ultimate displacement of the specimens. According to the analysis of ductility coefficient and ultimate displacement, a conclusion can be drawn that the increase of thread depth will reduce the deformation performance of the specimens. What is more, the increase of thread depth mainly affects the deformation performance of bolts during the bolt force transmission stage and failure stage.

The comparison of the ultimate displacement of the specimens with different bolt diameters is shown in Fig. 15 and Table 4. The results indicate that the average ultimate displacements of M20 and M18 are 40% larger than those of M16 and M14. The test results show that the increase of bolt diameter can enhance the ultimate displacement. In addition, the average ultimate displacement of the specimens with bolt strength grade of 10.9 is 17% less than that of the specimens with bolt strength grade of 8.8. The analysis of ductility coefficient and ultimate displacement shows that the increase of the bolt grade will reduce the deformation performance of bolted connections. Moreover, the data show that surface treatment has little effect on the ultimate displacement of bolted connections.

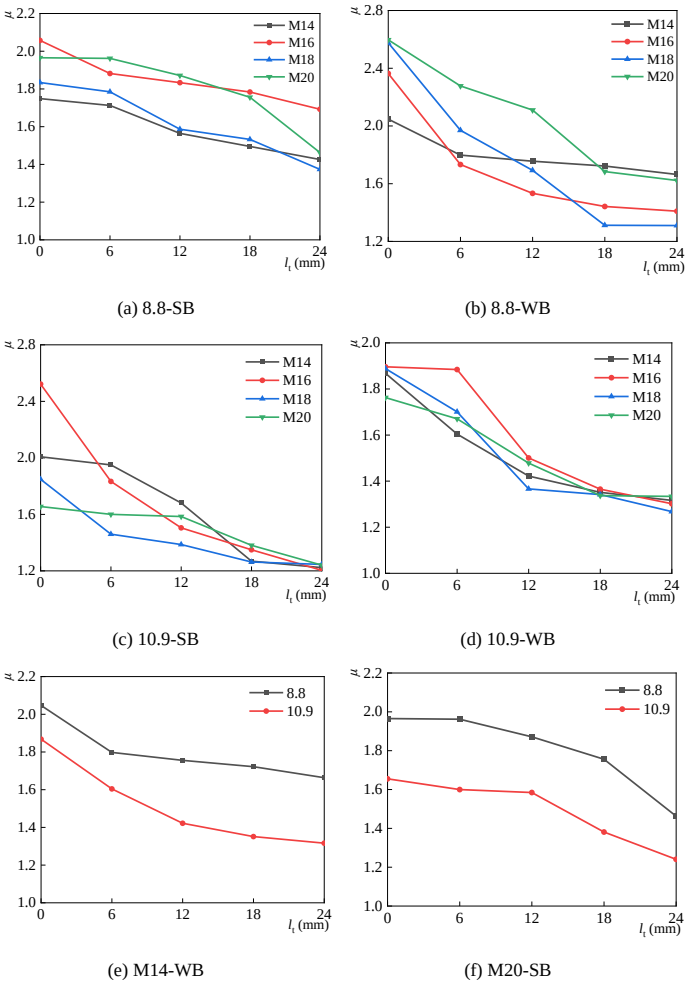

(a) 8.8-SB (b) 8.8-WB

(c) 10.9-SB (d) 10.9-WB

(e) M14-WB (f) M20-SB

Fig. 14 Ductility coefficient versus thread depth curves

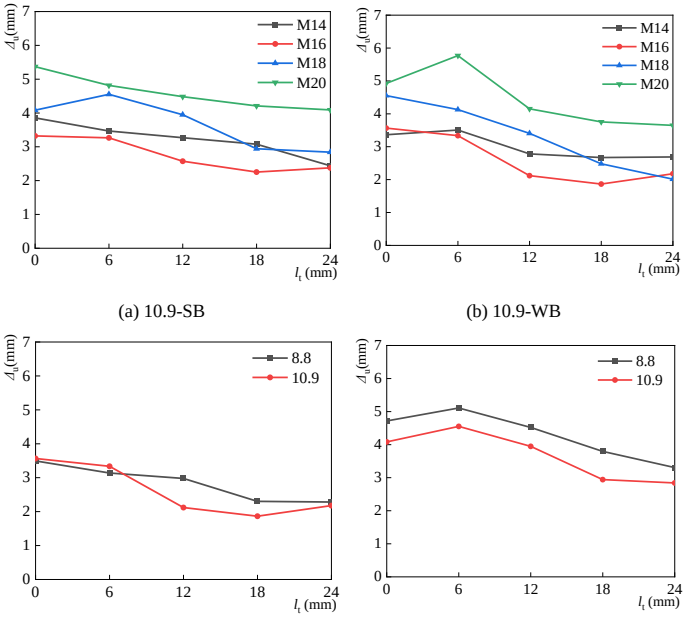

(a) 10.9-SB (b) 10.9-WB

(c) M16-WB (d) M18-SB

Fig. 15 Ultimate displacement versus thread depth curves

3.8. Strain distribution of plate

To assess the strain characteristics of bolted connections, the strain around the hole wall of the plate was acquired through the strain rosettes on six measuring points. The strain intensity of T1-T6 measuring points was calculated according to the following formula [29]:

$$\varepsilon_i = \frac{\sqrt{2}}{3}\sqrt{(\varepsilon_1-\varepsilon_2)^2+(\varepsilon_2-\varepsilon_3)^2+(\varepsilon_3-\varepsilon_1)^2} \tag{3}$$

where ε_1, ε_2, and ε_3 are the three directional principal strains, respectively.

Fig. 16 indicates the strain intensity of the six measuring points of the typical specimens under different load levels. The horizontal coordinate in the figure is the number of the strain rosettes, and the vertical coordinate ε_i is the strain intensity. The results indicate that the strain intensity of the six measuring points increases as the load increases, and when the load is less than 60% of the maximum load, the strain intensity of the six measuring points is approximately uniform. However, as the load exceeds 60% of the maximum load, the strain intensity distribution is no longer uniform. When the load reaches the ultimate bearing capacity, the strain intensity of measured points T1 and T6 are similar and larger among the six measuring points, and the strain intensity of measuring points T2, T3, T4, and T5 are smaller. In addition, the strain intensity of the measuring points T1 and T6 increases significantly at the ultimate bearing capacity. At this time, the strain intensity of measuring points T2, T3, T4, and T5 also increases, but the rate of increase is much smaller than that of the measuring points T1 and T6.

The influence of the thread depth on the strain intensity of the six measuring points is presented in Fig. 16. It is observed that the strain intensity distribution patterns of M18-8.8-SB-24-0, M18-8.8-SB-24-12, and M18-8.8-SB-24-24 are roughly the same. As the thread depth gradually increases, the ultimate bearing capacity of the specimens decreases gradually, and the strain intensity at the ultimate bearing capacity also decreases gradually. When the thread depth changes from 0mm to 12mm, the strain intensity of the measuring points T1 and T6 at the ultimate bearing capacity decreases significantly. Moreover, when the thread depth changes from 12mm to 24mm, the strain intensity of the measuring points T1 and T6 decreases slightly.

Fig. 16 (b) and (g) show that the effect of surface treatment on the strain intensity of the specimens. The results indicate that the strain intensity distribution patterns of the two specimens are roughly the same. By comparing the strain intensity of the measured points T1 and T6 at the maximum load, it is observed that the strain intensity of the specimens with the wire-brushed surface is higher.

The effect of bolt diameter on the strain intensity of bolted connections is illustrated in Fig. 16 (b), (d), (e), and (f). When the bolt diameter increases from M14 to M20, the ultimate bearing capacity of bolted connections gradually increases, and the strain intensity of the measurement points T1 and T6

increases obviously. For specimen M14-8.8-SB-24-12, due to the relatively small ultimate bearing capacity, there is no phenomenon that the strain intensity of the measured points T1 and T6 is large, and the strain intensity of all the measured points is small. According to Fig. 16 (b) and (h), if the bolt grade ranges from 8.8 to 10.9, the strain intensity of the measuring points T1 and T6 increases significantly. Moreover, it can be found that the changes of thread depth, surface treatment, bolt diameter, and bolt strength grade have no significant effect on the strain intensity of the measuring points T2, T3, T4, and T5.

When the specimen is in the bolt force transmission stage, the bolt contacts the hole wall, and the hole wall is squeezed. In this test, the bolt squeezes the hole wall close to the measuring points T1 and T6. It can be inferred that the location of the maximum strain intensity of the plate is the hole wall the extruded by the bolt, and the strain intensity of other hole wall areas is very small.

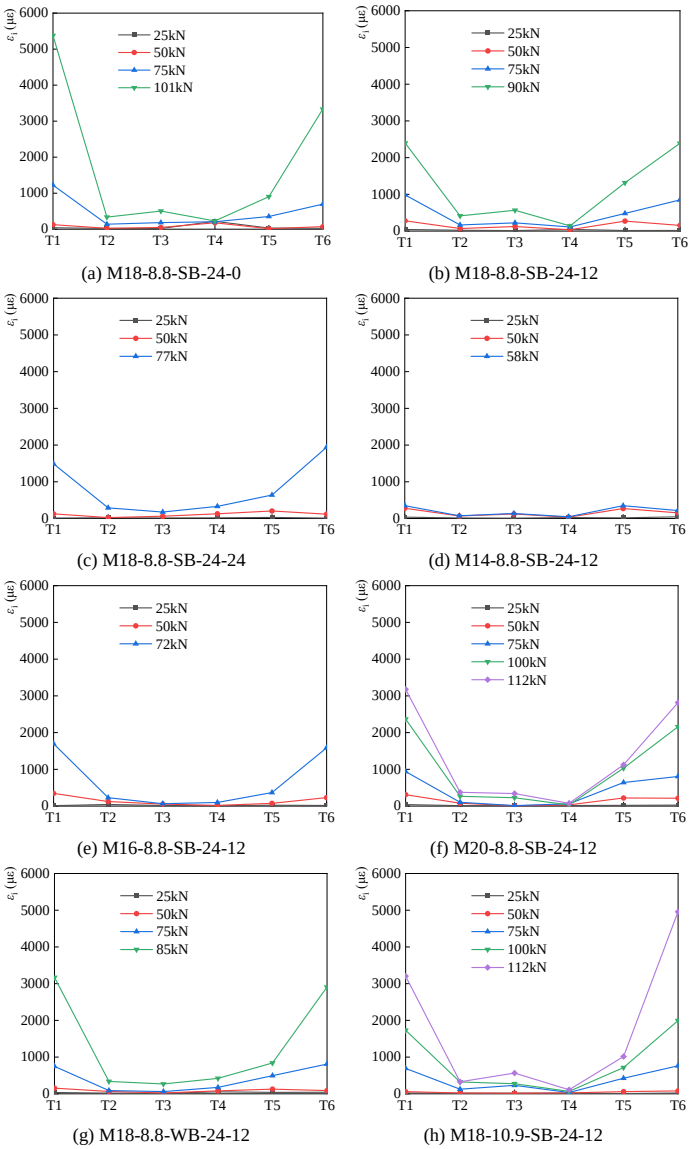

(a) M18-8.8-SB-24-0 (b) M18-8.8-SB-24-12

(c) M18-8.8-SB-24-24 (d) M14-8.8-SB-24-12

(e) M16-8.8-SB-24-12 (f) M20-8.8-SB-24-12

(g) M18-8.8-WB-24-12 (h) M18-10.9-SB-24-12

Fig. 16 Strain intensity distribution

4. Parametric formulas

4.1. Existing research

Currently, there are many researches on bolt design method, which effectively promotes the establishment of calculation formula in design specifications. Eurocode3 [30] and AISC [31] put forward formulas related to the shear capacity of bolts. Bolt shear design value formulas in the specification are shown in Eqs. (4) and (5).

$$F_{\mathrm{V,Rd}} = \frac{\alpha_{\mathrm{v}} f_{\mathrm{ub}} A}{\gamma_{\mathrm{M2}}} \tag{4}$$

where γ_{M2} is the partial coefficient of resistance, γ_{M2}=1.25, f_{ub} is ultimate tensile strength. When the shear surface passes through the threaded section, A is tensile stress zone: in this case, for bolts of strength class 8.8, α_v=0.6, for bolts of strength class 10.9, α_v=0.5. When the shear surface passes through the unthreaded section, A is the total gross cross-section, α_v=0.6.

$$R_{\mathrm{n}} = \varphi F_{\mathrm{nv}} A_{\mathrm{b}} \tag{5}$$

where φ is the reduction factor, φ=0.75. A_b is the nominal cross-sectional area of the bolt, F_{nv} is the nominal shear strength of the high-strength bolt. When the shear surface passes through the threaded section, F_{nv}=0.450F_{ub} (F_{ub} is the nominal tensile strength of the bolt), and when the shear surface passes through the unthreaded section, F_{nv}=0. 563F_{ub}.

4.2. Establishment of design formula

AISC defines the design value of bolt shear strength according to whether there are threads in the shear plane, and the bolt cross-section area is calculated according to the nominal diameter of the bolt. Eurocode3 defines the design value of shear strength and the area of the bolt cross-section according to whether there are threads in the shear plane. The ultimate bearing capacity of bolted connections obtained from the test result was compared with the formulas of the above design code, as plotted in Table 5. It is observed that the ultimate bearing capacity of bolted connections with shot-blasted surfaces is larger than that of bolted connections with wire-brushed surfaces. However, the above two formulas do not consider the influence of surface treatment, so both of these design methods can not accurately predict the ultimate bearing capacity of bolts. In order to better predict the ultimate bearing capacity, the friction force of the bolted connection cannot be neglected. Therefore, the ultimate bearing capacity design formula as controlled by the shear strength of the bolts is initially defined as

$$P_1 = 0.9 \times \mu \times n_{\mathrm{v}} \times P + n_{\mathrm{v}} \times \frac{\pi}{4} \times d^2 \times f_{\mathrm{v}}^{\mathrm{b}} \tag{6}$$

where n_v is the number of shear surfaces, μ is the slip coefficient of the friction surface (the slip coefficient of the shot-blasted surfaces is 0.45, and that of the wire-brushed surfaces is 0.30), P is the design value of bolt pre-tension, d is the bolt diameter (when the shear plane is at the thread, select the effective diameter for calculation), f_v^b is the design value of the shear strength of the bolt. The "$0.9\times\mu\times n_v\times P$ " represents the friction between the plates and the " $n_v\times\pi/4\times d^2\times f_v^b$ " represents the shearing capacity of the bolt.

The concept of this formula is relatively clear, which shows that the ultimate bearing capacity of a bolted connection consists of the shear load capacity of the bolt and the friction resistance between the plates. Fig. 17 includes the calculated value (P_{cu}) and experimental value (P_{eu}) of the above three formulas. The diagonal line in Fig. 17 represents that the calculated value of the formula is equal to the experimental value. The accuracy of the formula can be judged by the degree of deviation of each point from the diagonal line. The ultimate bearing capacity of the specimens is lower than the calculated values of AISC design method and Eurocode 3 design method, and the calculated values of the specimens with the slip coefficient of 0.45 deviates greatly from the experimental results.

Eqs. (6) considers the shear bearing capacity of the bolts and the friction resistance between the plates, and it is more accurate to calculate the ultimate bearing capacity of specimens with different slip coefficients. However, the consideration of thread depth in Eqs. (4)-(6) only includes two cases (the shear surface passes through the threaded section or not), and the influence of thread depth is not considered quantitatively. Therefore, thread depth reduction factor ($f(d_t)$) was adopted to consider the adverse effect of the thread depth on the ultimate bearing capacity. Thus, the form of the ultimate bearing capacity of the high-strength bolt is as follows:

$$P_{\mathrm{NEW}} = \alpha_1 \times 0.9 \times \mu \times n_{\mathrm{v}} \times P + \alpha_2 \times f\left(d_{\mathrm{t}}\right) \times n_{\mathrm{v}} \times \frac{\pi}{4} \times d^2 \times f_{\mathrm{v}}^{\mathrm{b}} \tag{7}$$

$$d_{\mathrm{t}} = \frac{l_{\mathrm{t}}}{l_{\mathrm{h}}} \tag{8}$$

where $f(d_t)$ is a function of d_t, d_t is the ratio of thread depth, l_t is the thread depth

value, l_h is the total depth of the bolt hole. α_1 and α_2 are adjustment coefficients.

Then, according to the test results, the calculation formula of $f(d_t)$ and the adjustment coefficients α_1 and α_2 were obtained through Origin2018 software. The formula is as follows:

$$f\left(d_t\right)=1-0.196\times d_t \tag{9}$$

$$P_{NEW}=1.133\times 0.9\times \mu\times n_v\times P+0.956\times\left(1-0.279\times d_t\right)\times n_v\times\frac{\pi}{4}\times d^2\times f_v^b \tag{10}$$

Table 5
Comparison of ultimate strength with AISC-360, Eurocode 3 and proposed formula

Specimen label	d_t	P_{eu}	P_{AISC}	P_{EU3}	P_{NEW}	P_{AISC}/P_{eu}	P_{EU3}/P_{eu}	P_{NEW}/P_{eu}
M14-8.8-WB-24-0	0.00	60	54	59	58	0.90	0.99	0.97
M14-8.8-WB-24-6	0.25	57	54	59	56	0.95	1.04	0.98
M14-8.8-WB-24-12	0.50	53	43	44	45	0.81	0.83	0.84
M14-8.8-WB-24-18	0.75	48	43	44	43	0.89	0.91	0.89
M14-8.8-WB-24-24	1.00	43	43	44	41	0.99	1.02	0.95
M14-8.8-SB-24-0	0.00	65	54	59	64	0.83	0.91	0.99
M14-8.8-SB-24-6	0.25	62	54	59	62	0.87	0.95	0.99
M14-8.8-SB-24-12	0.50	58	43	44	51	0.74	0.76	0.88
M14-8.8-SB-24-18	0.75	53	43	44	49	0.81	0.83	0.93
M14-8.8-SB-24-24	1.00	49	43	44	47	0.89	0.91	0.97
M14-10.9-WB-24-0	0.00	72	68	74	72	0.94	1.03	1.01
M14-10.9-WB-24-6	0.25	70	68	74	69	0.97	1.06	0.99
M14-10.9-WB-24-12	0.50	63	54	46	56	0.86	0.73	0.90
M14-10.9-WB-24-18	0.75	58	54	46	54	0.93	0.79	0.93
M14-10.9-WB-24-24	1.00	52	54	46	51	1.04	0.89	0.99
M14-10.9-SB-24-0	0.00	82	68	74	80	0.82	0.90	0.97
M14-10.9-SB-24-6	0.25	78	68	74	77	0.87	0.95	0.99
M14-10.9-SB-24-12	0.50	74	54	46	64	0.73	0.62	0.86
M14-10.9-SB-24-18	0.75	65	54	46	61	0.84	0.71	0.95
M14-10.9-SB-24-24	1.00	54	54	46	59	1.00	0.85	1.09
M16-8.8-WB-24-0	0.00	76	71	77	77	0.93	1.02	1.01
M16-8.8-WB-24-6	0.25	72	71	77	73	0.98	1.07	1.02
M16-8.8-WB-24-12	0.50	66	56	60	61	0.85	0.91	0.92
M16-8.8-WB-24-18	0.75	59	56	60	58	0.95	1.01	0.98
M16-8.8-WB-24-24	1.00	56	56	60	56	1.00	1.08	0.99
M16-8.8-SB-24-0	0.00	88	71	77	85	0.80	0.88	0.97
M16-8.8-SB-24-6	0.25	81	71	77	81	0.87	0.95	1.00
M16-8.8-SB-24-12	0.50	76	56	60	69	0.74	0.80	0.91
M16-8.8-SB-24-18	0.75	66	56	60	66	0.86	0.92	1.01
M16-8.8-SB-24-24	1.00	64	56	60	64	0.88	0.94	1.00
M16-10.9-WB-24-0	0.00	93	88	97	95	0.95	1.04	1.03
M16-10.9-WB-24-6	0.25	87	88	97	91	1.02	1.11	1.05
M16-10.9-WB-24-12	0.50	80	71	63	76	0.88	0.78	0.95
M16-10.9-WB-24-18	0.75	70	71	63	73	1.01	0.90	1.04
M16-10.9-WB-24-24	1.00	64	71	63	69	1.11	0.98	1.09
M16-10.9-SB-24-0	0.00	101	88	97	105	0.88	0.96	1.05
M16-10.9-SB-24-6	0.25	98	88	97	101	0.90	0.99	1.04
M16-10.9-SB-24-12	0.50	88	71	63	86	0.80	0.71	0.97
M16-10.9-SB-24-18	0.75	79	71	63	83	0.89	0.79	1.04
M16-10.9-SB-24-24	1.00	74	71	63	79	0.95	0.84	1.07
M18-8.8-WB-24-0	0.00	95	89	98	96	0.93	1.02	1.01
M18-8.8-WB-24-6	0.25	90	89	98	92	0.99	1.09	1.03
M18-8.8-WB-24-12	0.50	85	71	74	75	0.84	0.87	0.88
M18-8.8-WB-24-18	0.75	78	71	74	72	0.92	0.95	0.93
M18-8.8-WB-24-24	1.00	70	71	74	69	1.01	1.06	0.98

M18-8.8-SB-24-0	0.00	101	89	98	107	0.88	0.97	1.06
M18-8.8-SB-24-6	0.25	96	89	98	102	0.93	1.02	1.07
M18-8.8-SB-24-12	0.50	90	71	74	86	0.79	0.82	0.95
M18-8.8-SB-24-18	0.75	85	71	74	82	0.84	0.88	0.98
M18-8.8-SB-24-24	1.00	77	71	74	79	0.92	0.96	1.03
M18-10.9-WB-24-0	0.00	122	112	122	118	0.92	1.00	0.97
M18-10.9-WB-24-6	0.25	117	112	122	113	0.95	1.04	0.96
M18-10.9-WB-24-12	0.50	105	89	77	92	0.85	0.73	0.87
M18-10.9-WB-24-18	0.75	92	89	77	88	0.97	0.84	0.96
M18-10.9-WB-24-24	1.00	86	89	77	84	1.03	0.89	0.97
M18-10.9-SB-24-0	0.00	131	112	122	130	0.85	0.93	0.99
M18-10.9-SB-24-6	0.25	126	112	122	125	0.89	0.97	1.00
M18-10.9-SB-24-12	0.50	112	89	77	104	0.80	0.69	0.93
M18-10.9-SB-24-18	0.75	101	89	77	100	0.88	0.76	0.99
M18-10.9-SB-24-24	1.00	92	89	77	96	0.97	0.84	1.04
M20-8.8-WB-24-0	0.00	116	110	121	120	0.95	1.04	1.03
M20-8.8-WB-24-6	0.25	112	110	121	114	0.98	1.08	1.02
M20-8.8-WB-24-12	0.50	102	88	94	95	0.86	0.92	0.93
M20-8.8-WB-24-18	0.75	88	88	94	91	1.00	1.06	1.03
M20-8.8-WB-24-24	1.00	80	88	94	87	1.10	1.17	1.08
M20-8.8-SB-24-0	0.00	128	110	121	132	0.86	0.94	1.03
M20-8.8-SB-24-6	0.25	123	110	121	127	0.89	0.98	1.03
M20-8.8-SB-24-12	0.50	109	88	94	108	0.80	0.86	0.98
M20-8.8-SB-24-18	0.75	101	88	94	104	0.87	0.93	1.03
M20-8.8-SB-24-24	1.00	92	88	94	100	0.95	1.02	1.08
M20-10.9-WB-24-0	0.00	146	138	151	148	0.94	1.03	1.02
M20-10.9-WB-24-6	0.25	142	138	151	142	0.97	1.06	1.00
M20-10.9-WB-24-12	0.50	122	110	98	118	0.91	0.81	0.97
M20-10.9-WB-24-18	0.75	113	110	98	113	0.98	0.87	1.00
M20-10.9-WB-24-24	1.00	108	110	98	108	1.02	0.90	0.99
M20-10.9-SB-24-0	0.00	161	138	151	164	0.86	0.94	1.02
M20-10.9-SB-24-6	0.25	157	138	151	158	0.88	0.96	1.01
M20-10.9-SB-24-12	0.50	133	110	98	134	0.83	0.74	1.01
M20-10.9-SB-24-18	0.75	123	110	98	129	0.89	0.80	1.04
M20-10.9-SB-24-24	1.00	116	110	98	124	0.95	0.84	1.06
Mean						0.91	0.92	0.99
Maximum						1.11	1.17	1.09
Minimum						0.73	0.62	0.84
Variance						0.006	0.013	0.003

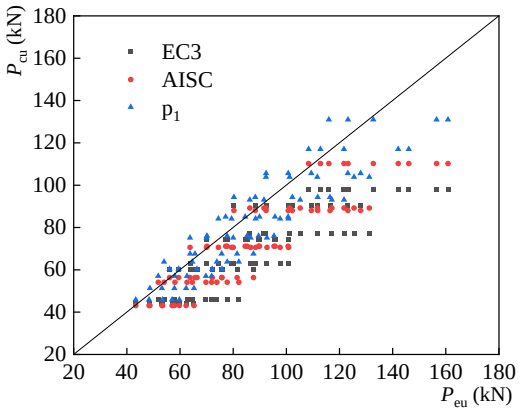

Fig. 17 Comparison of experimental results and formula value.

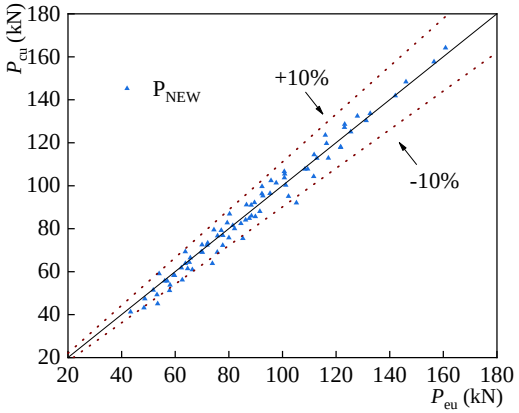

Fig. 18 Comparison with experimental results.

4.3. Verification of the design formula

To validate the accuracy of the design formula, the calculated value (P_{cu}) was compared with the experimental value (P_{eu}). The results of P_{cu}/P_{eu} are shown in Fig. 17 and Table 5. It can be observed that P_{cu}/P_{eu} of most specimens is between 0.9 and 1.1, which indicates that the design formula has a higher degree of accuracy. Compared with the original formula, the design formula also considers the friction force and thread depth.

The mean value of P_{cu}/P_{eu} is 0.99, the maximum value is 1.09, the minimum value is 0.84 and the variance is 0.003. The verification shows that the design formula for predicting the ultimate bearing capacity controlled by the shear strength of bolts is reasonable and accurate.

5. Conclusions

This paper experimentally investigated the mechanical behavior of the grade 8.8 and 10.9 small-sized (M14-M20) bolts with the thread into the bolt hole. The effects of the thread depth, surface treatment, bolt diameter, and bolt strength grade were studied. On the basis of the experimental results and modified formula, some conclusions can be drawn:

(1) Bolt shear failure is the typical failure mode. The bolt is subjected to the maximum tangential stress at the contact surface of the two connecting plates. The failure surface passes through the contact surface of the two plates. If the thread passes through the shear surface, the failure surface is along the direction of the thread, and the bolt failure surface is relatively rough.

(2) The initial stiffness does not vary significantly with the increase of the thread depth. The increase of thread depth has no obvious effect on the initial slip load, and surface treatment methods have a noticeable influence on the initial slip load.

(3) The trends of the displacement-load curves of bolted connections are approximately the same. The ultimate bearing capacity gradually decreases as the depth of thread extension into the hole increases. The enhancement of the contact surface roughness of the plate generally results in a noticeable reduction of the ultimate bearing capacity. Moreover, the diameter and strength grade of the bolt also affect the ultimate bearing capacity of bolted connections.

(4) The increase of the thread depth will reduce the ductility and ultimate displacement of bolted connections. The increase of bolt strength grade results in a decrease in the ductility of the specimen. Moreover, the increment in thread depth has an adverse effect on the yield load of bolted connections, and the contact surface treatment method, bolt diameter, and strength grade also influence the yield load of bolted connections.

(5) According to the test results, a design formula for predicting the ultimate bearing capacity considering the effect of thread depth is proposed. By comparing the calculation results with the experimental results, it is proved that the formula has better accuracy.

6. Acknowledgements

The authors wish to acknowledge funding supported by the National Natural Science Foundation of China (No. 52078138), the Science and Technology Planning Project of Fuzhou (No. 2020-GX-23), and the Natural Science Foundation of Fujian Province (No. 2020J01886)

References

[1] W. Lin, T. Yoda, Chapter seven-steel bridges, Bridg. Eng. (2017) 111-136.
[2] G.L. Kulak, J.W. Fisher, J.H.A. Struik, Guide to design criteria for bolted and riveted joints 2nd ed, American Institute of Steel Construction, Chicago, IL, 2001.
[3] Z.W. Jiang, S. Wan, Z. Fang, et al., Static and fatigue behaviours of a bolted GFRP/steel double lap joint, Thin-Walled Struct. 158 (2021), 107170.
[4] B. Qiu, X. Yang, Z. Zhou, et al., Experimental study on fatigue performance of M30 high-strength bolts in bolted spherical joints of grid structures, Eng Struct. 205 (2020), 110123.
[5] H.J. Kim, J.A. Yura, The effect of ultimate-to-yield ratio on the bearing strength of bolted connections, J. Constr. Steel Res. 49 (3) (1999) 255-269.
[6] C.O. Rex, W.S. Easterling, Behavior and modeling of a bolt bearing on a single plate, J. Struct. Eng. 129 (6) (2003) 792-800.
[7] G.L. Kulak, G.Y. Grondin, Block shear failure in steel members-a review of design practice, American Institute of Steel Construction, 38 (4) (2001) 199-203.
[8] Y.J. Shi, M. Wang, Y.Q. Wang, Analysis on shear behavior of high-strength bolts connection, Int. J. Steel. Struct. 11 (2) (2011) 203-213.
[9] C.D. Annan, A. Chiza, Characterization of slip resistance of high strength bolted connections with zinc-based metallized faying surfaces, Eng Struct. 56 (2013) 2187-2196.
[10] C.D. Annan, A. Chiza, Slip resistance of metalized-galvanized faying surfaces in steel bridge construction, J. Constr. Steel Res. 95 (2014) 211-219.
[11] Y.B. Wang, Y.F. Lyu, G.Q. Li, et al., Behavior of single bolt bearing on high strength steel plate, J. Constr. Steel Res. 137 (2017) 19-30.
[12] A. Cruz, R. Simoes, R. Alves, Slip factor in slip resistant joints with high strength steel, J. Constr. Steel Res. 70 (2012) 280-288.
[13] C. Stocchi, P. Robinson, S.T. Pinho, A detailed finite element investigation of composite bolted joints with countersunk fasteners, Compos Part A-Appl S. 52 (2013) 143-150.
[14] T.S. Kim, H. Kuwamura, S.H. Kim, Y.T. Lee, T.J. Cho, Investigation on ultimate strength of thin-walled steel single shear bolted connections with two bolts using finite element analysis, Thin-Wall Struct. 47 (11) (2009) 1191-1202.
[15] Z.G Xu, Q. Chen, C.G. Deng, R.Y. Chen, Analysis of bearing capacities of connections with some threads inserted into the bolt hole, Progress in Steel Building Structures. China, 2019 (in Chinese).
[16] A. Ahmed, L.H. Teh, Thread effects on the stiffness of bolted shear connections, J. Constr. Steel Res. 160 (2019) 77-88.
[17] GB/T 5277-1985, Fasteners-Clearance holes for bolts and screws, Beijing, 1985 (In Chinese).
[18] Y.F. Lyu, G.Q. Li, Y.B. Wang, H. Li, Y.Z. Wang, Bearing behavior of multi-bolt high strength steel connections, Eng Struct. 212 (2020), 110510.
[19] P. Može, D. Beg, J. Lopatič. Net cross-section design resistance and local ductility of elements made of high strength steel, J. Constr. Steel Res. 63 (11) (2007) 1431-1441.
[20] T.S. Kim, H. Kuwamura, T.J. Cho, A parametric study on ultimate strength of single shear bolted connections with curling, Thin-Walled Struct. 46 (1) (2008) 38-53.
[21] GB 50017-2017, Code for Design of Steel Structure, Beijing, 2017 (in Chinese).
[22] GB/T 2975-2018, Steel and steel products-Location and preparation of samples and test pieces for mechanical testing, Beijing, 2018 (in Chinese).
[23] GB/T 228.1-2010, Metallic materials-Tensile testing-Part 1: Method of test at room temperature, Beijing, 2010 (in Chinese).
[24] Z. Guo, L.J. Xia, Y. Chen, et al., Test on mechanical behavior of pultruded concrete-filled GFRP tubular short columns after elevated temperatures, Compos. Struct. 257 (2021), 113163.
[25] Z. Guo, Y. Zhu, Y. Chen, et al., Test on residual ultimate strength of pultruded concrete-filled GFRP tubular short columns after lateral impact, Compos. Struct. 260 (2021), 113520.
[26] Z. Guo, Y. Chen, Y. Wang, Experimental study on square concrete-filled double skin steel tubular short columns, Thin-Walled Struct. 156 (2020), 107017.
[27] Z.H. Guo, X.D. Shi, Theory and analysis of reinforced concrete, Tsinghua University Press. (2003) 163-337 (in Chinese).
[28] P. Feng, H.L Qiang, L.P Ye, Discussion and definition on yield points of materials, members and structures, Engineering Mechanics, 34 (3) (2017) (in Chinese).
[29] Y. Kurobane, Y. Makino, K. Ochi, Ultimate resistance of unstiffened tubular joints, J. Struct. Eng. 110 (2) (1984) 385-400.
[30] CEN, Eurocode 3: Design of steel structures, part 1-1: general rules and rules for buildings, EN 1993-1-1, European Committee for Standardization, Brussels, 2005.
[31] American Institute of Steel Construction, Specification for structural steel building, AISC 360-16, Chicago, IL, 2016.